International Journal of Nanomedicine

Dovepress
Taylor & Francis Group

Open Access Full Text Article

ORIGINAL RESEARCH

Engineered Cancer Cell Membrane-Functionalized Metal-Organic Frameworks for Irinotecan/Curcumin Codelivery in Colorectal Cancer: Enhanced Efficacy and Mitigated Toxicity

Shuiling Jin[1,*], Aifang Zhou[2,*], Qi Zhang[1,*], Di Zhao[2], Xintong Dong[2], Hong-Min Meng[2], Zhengquan Yu[1], Zhaohui Li[1]

[1]The First Affiliated Hospital of Zhengzhou University, Zhengzhou, Henan Province, People's Republic of China; [2]College of Chemistry, Zhengzhou University, Zhengzhou, Henan Province, People's Republic of China

*These authors contributed equally to this work

Correspondence: Hong-Min Meng, College of Chemistry, Zhengzhou University, Zhengzhou, Henan Province, People's Republic of China, 450001, Email hmmeng2017@zzu.edu.cn; Zhaohui Li, The First Affiliated Hospital of Zhengzhou University, Zhengzhou, Henan Province, People's Republic of China, 450052, Email zhaohui.li@zzu.edu.cn

Purpose: Irinotecan (CPT-11), a semisynthetic camptothecin derivative and topoisomerase I inhibitor, is globally used for treating cancers such as colorectal cancer. However, its clinical application is limited by severe adverse effects, including diarrhea and myelosuppression. Biomimetic nano-drug delivery is widely used and can improve chemotherapeutic activity and decrease side effects.

Methods: In this study, we developed a cancer cell membrane-functionalized metal-organic frameworks for irinotecan/curcumin (named MZCC) for colorectal cancer treatment. In this study, by combining irinotecan, curcumin, MOFs and functionalized cancer cell membrane, a pH-sensitive drug delivery system of MZCC was developed for colorectal cancer treatment with enhanced chemotherapeutic efficacy while reducing side effects. The characteristics and stability of MZCC were carefully examined, and its anti-cancer efficiency was studied in vitro and in vivo. In vivo experiments in a murine colorectal cancer mouse model given intratumorally MZCC injection every 4 days were used to assess antitumor efficacy and systemic toxicity.

Results: The MZCC system improved treatment antitumor efficacy by 2.3-fold compared with free CPT-11 through synergistic chemotherapy. MZCC-treated groups exhibited a significant reduction in inflammatory cytokine levels within colon tissues; inflammation levels decreased by 55% compared with free CPT-11, and colon length was restored to 79% of normal.

Conclusion: Our strategy effectively alleviates CPT-11-induced intestinal toxicity and mitigates adverse reactions. This approach may provide a novel method for enhancing chemotherapeutic efficacy while reducing gastrointestinal toxicity.

Keywords: colorectal cancer, irinotecan, curcumin, metal-organic frameworks, cell membrane

Introduction

Colorectal cancer (CRC), the third most common cancer globally and the second leading cause of cancer-related deaths,[1] is commonly treated with surgery, radiotherapy, and chemotherapy.[2–6] However, since surgery and radiotherapy are often not viable options for most patients with advanced CRC, chemotherapy becomes essential for controlling disease progression and improving quality of life. Key chemotherapeutic agents include irinotecan (CPT-11) and its active metabolite 7-ethyl-10-hydroxy-camptothecin.[7–9] Unfortunately, these drugs also induce cytotoxic effects in epithelial cells, hematopoietic cells, and commensal bacteria, leading to significant toxic side effects such as gastrointestinal toxicity (nausea, vomiting, and diarrhea).[10–12] In addition, they also may cause inflammatory responses and chemokine upregulation, leading to treatment resistance and tumor recurrence, thus limiting their effectiveness. These adverse

Received: 6 August 2025
Accepted: 12 November 2025
Published: 19 November 2025

Graphical Abstract

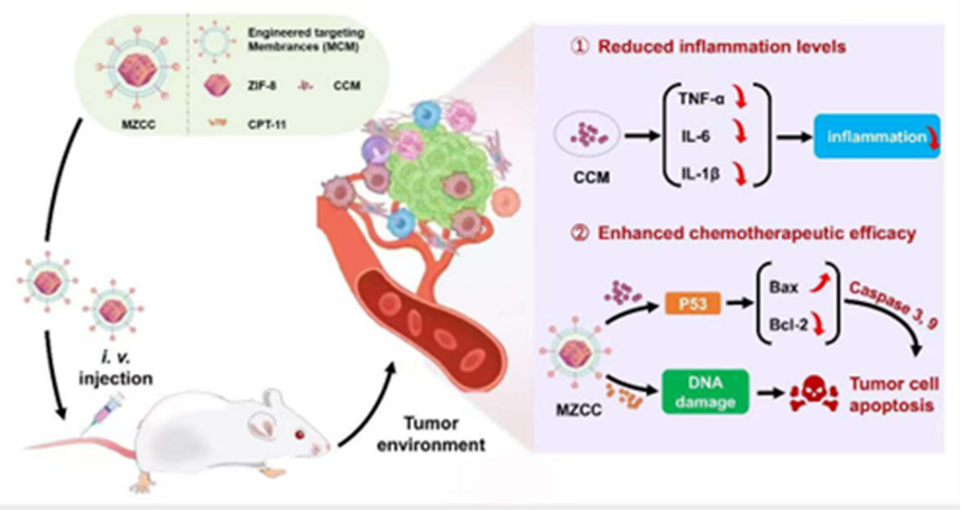

effects frequently necessitate reducing the dosage or frequency of CPT-11 administration, severely limiting its use to a minority of CRC patients with good performance status. Consequently, strategies to mitigate CPT-11 toxicity are urgently needed to enhance its utility as a first-line therapy for CRC.

Natural products are a major focus in antitumor drug discovery because of their well-documented efficacy and vast resource potential.[13,14] They are often perceived as safer with fewer side effects, and possess beneficial properties such as immune enhancement and chemo-sensitization. Synergistic combination therapy incorporating natural chemosensitizers is a promising emerging strategy to overcome multidrug resistance and mitigate the side effects of conventional chemotherapeutics. Curcumin, a polyphenolic compound derived from turmeric (a traditional Chinese medicine), exhibits diverse beneficial effects, including antitumor, antioxidant, antiviral, and antimutagenic activities.[15–17] Therefore, exploring the combination of curcumin with the commonly used chemotherapeutic agent CPT-11 for CRC treatment merits carefully investigation.

In recent years, significant attention has been drawn to nanocarrier-mediated drug delivery platforms—including polymeric micelles, liposomes, and hybrid organic-inorganic nanoparticles—due to their distinct physicochemical characteristics in cancer treatment.[18–20] Metal-organic frameworks (MOFs) have gained recognition as highly promising drug carriers, facilitating therapeutic loading via either physical encapsulation or chemical conjugation strategies.[21–23] Because of their large porosity and hydrophobic voids, MOFs have a higher drug loading capacity than traditional carriers.[24–26] Their controlled host-guest interactions and biodegradability further enhance their appeal for drug delivery applications.[27–30] Additionally, surface functionalization is a well-established strategy for improving MOFs biocompatibility and targeting.[31–33] Biomimetic nano-drug delivery systems typically comprise a drug-loaded core nanostructure and an outer biomimetic membrane with biological activity.[34–37] A novel approach utilizing coatings derived from biomimetic materials has revolutionized nanocarriers functionalization, involving transferring plasma membranes from native cells onto synthetic nanocarriers.[38–42] The resulting biomimetic material-coated nanocarriers retain the complex surface characteristics of their source cells and acquire cell-mimicking functionalities. Extensive research has been conducted on diverse biomimetic nanoparticle-coated formulations, demonstrating their significant promise for therapeutic delivery applications.

The mannose receptor (MR) which is highly expressed on macrophages and CRC cell lines are promising therapeutic targets for cancer treatment via mediating receptor-specific endocytosis to enhance tumor accumulation.[43,44] Building on this finding, we engineered mannosylation cancer cell membrane (MCM)-coated zeolitic imidazole frameworks (ZIF-8)[45]

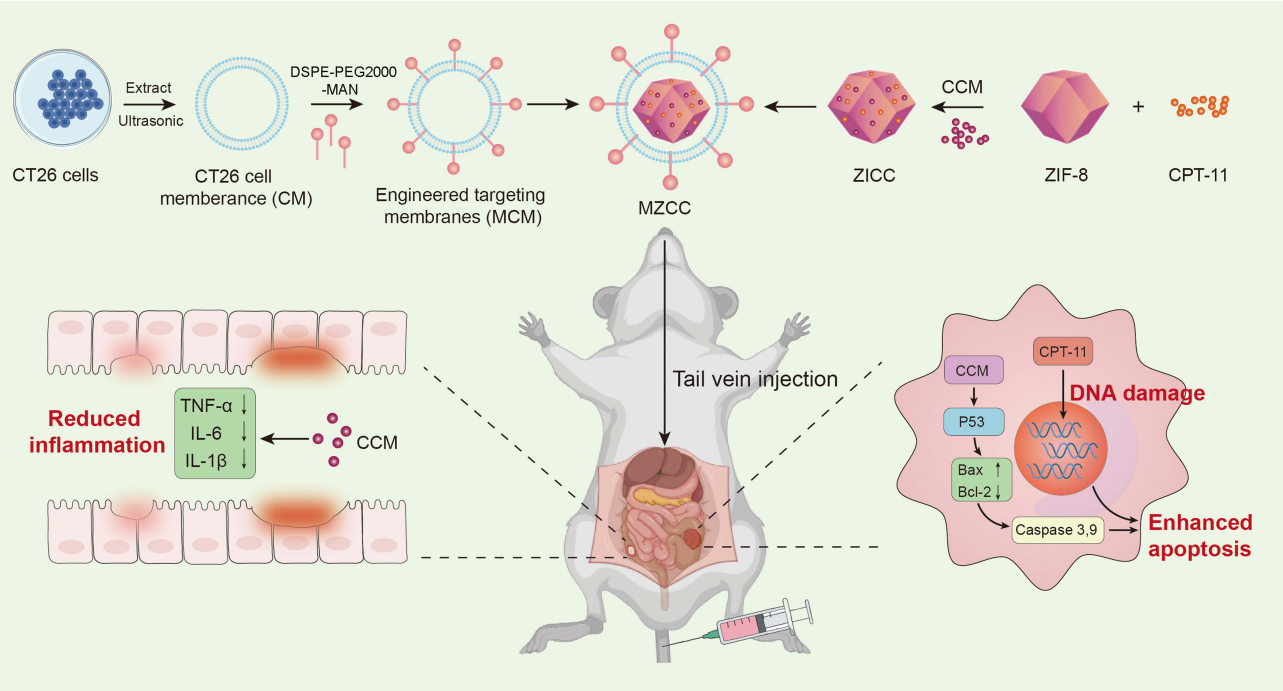

Figure 1 Schematic diagram of the preparation of MZCC and MZCC-induced antitumor and anti-inflammatory activity.

co-loading CPT-11 and curcumin (CCM) to prepare MZCC for CRC treatment to enhance the therapeutic efficacy of CPT-11 and reduce its systemic toxicity (Figure 1). This integrated nanoplatform concurrently addresses three critical objectives: immune evasion through biomimetic membrane camouflage, active targeting through mannose-receptor interactions, and controlled dual-drug release triggered by acidic tumor microenvironment. These advances represent a significant step toward next-generation drug delivery systems that maximize therapeutic efficacy while minimizing systemic toxicity.

Materials and Methods

Materials

Irinotecan was purchased from Aladdin Scientific Co., Ltd. (Shanghai, China). Curcumin was purchased from Macklin reagent Co., Ltd. (Shanghai, China). 2-methylimidazole, zinc nitrate hexahydrate and Rhodamine B were purchased from Sinopharm Chemical Co., Ltd (Shanghai, China). DMEM medium, PBS buffer, cell apoptosis kit, 0.25% trypsin and McCoy's medium was purchased from Servicebio Technology Co., Ltd (Wuhan, China). TNF-α ELISA kit, IL-6 ELISA kit and IL-1β ELISA kit were purchased from Enzyme-linked Biotechnology Co., Ltd (Shanghai, China). Commercial reagents including thiazolyl blue tetrazolium bromide (MTT) and an Annexin V-FITC/PI apoptosis detection kit were obtained from Sangon Biotech (Shanghai, China). For animal studies, female BALB/c mice were acquired from SPF Biotechnology (Beijing, China).

Methods

Characterization

Microstructural characterization was conducted using a JEM-2100 field emission TEM (JEOL, Japan) at an accelerating voltage of 200 kV. Particle size distribution and surface charge measurements were obtained with a Malvern Zeta-sizer Nano ZS90 instrument (England). The Hitachi U3900H system (Japan) was utilized for ultraviolet-visible absorption measurements. Fluorescence spectral analysis was conducted on a Hitachi F-7100 platform (Japan), with Fourier-transform infrared spectroscopy performed on Bruker's Tensor 27 instrument (Germany). Fluorescence imaging was performed on a Leica TCS SP8 laser scanning confocal microscope (Germany). The MTT-based cytotoxicity results were

https://doi.org/10.2147/IJN.S558675

quantified by a Spark® multimode plate reader from Tecan (Switzerland). Flow cytometry analysis was obtained via a Flow Cytometer (Beckman, USA). In vivo fluorescence images were obtained on an IVIS® Spectrum in vivo imaging system (PerkinElmer, USA).

Synthesis of ZIC

The synthesis of CPT-11@ZIF-8 (ZIC) followed a previously reported method. Initially, 20 mg of CPT-11 was dissolved in 400 μL of an aqueous solution containing 33.6 mg of 2-methylimidazole (2-MeIm). Next, 33.6 mg of zinc nitrate hexahydrate ($Zn(NO_3)_2 \cdot 6H_2O$) dissolved in 40 μL of water was added to the CPT-11/2-MeIm solution under vigorous stirring for 5 minutes. This reaction yielded a white ZIC precipitate. The product was isolated by centrifugation at 8000 rpm for 10 minutes and washed three times with water. For comparison, ZIF-8 without CPT-11 was also synthesized according to the similar method.

Synthesis of ZICC

CCM was conjugated to ZIC to prepare ZICC using the following procedure. First, 0.25 mg of CCM was dissolved in 1 mL of 95% ethanol and stirred for 2 hours to ensure complete dissolution. Subsequently, 10 mg of ZIC was added to the CCM solution. To facilitate CCM-ZIC conjugation, the solution was continuously agitated at 25°C for a 24-hour period. The resulting yellow precipitate (ZICC) was collected by centrifugation at 8500 rpm for 10 minutes.

In vitro Drug Release Studies

Experiments investigating pH-sensitive drug release for MZCC were performed under both physiological pH and acidic conditions (pH = 5.5, pH = 6.4, pH = 7.4) to mimic the acidic environment in tumor cells. At predetermined intervals, 1 mL samples were withdrawn and replaced with an equal volume of fresh PBS. The samples were then centrifuged, and the clear supernatant was analyzed using UV–vis spectroscopy to quantify CPT-11 or CCM.

In vitro Anticancer Study

Cell lines used in this work were provided by National Collection of Authenticated Cell Cultures (Shanghai, China). We cultured CT26 cells in DMEM enriched with 10% fetal bovine serum to investigate MZCC's in vitro antitumor effects, maintaining optimal growth conditions at 37°C with 5% CO_2 and high humidity. For the viability assay, CT26 cells were plated in a 96-well plate. After 48 hours of incubation, the medium was replaced with serially diluted solutions of the test compounds (ZIF-8, CPT-11, CCM, ZIC, ZICC, MZCC). Following an additional 24-hour incubation, cell viability was assessed using an MTT assay. Following addition of MTT reagent to all wells and subsequent 4-hour incubation, DMSO was used to solubilize the formed formazan crystals. Optical density measurements were then conducted at 540 nm with a microplate reader. Cell viability was determined from the absorbance values, and the percentage growth inhibition was calculated relative to untreated controls.

Apoptosis Assay

For the cell apoptosis assay, CT26 cells (3×10^5 cells per well) were incubated for 24 hours with PBS (control), CPT-11 (16 μg/mL), CCM (5.2 μg/mL), ZIC (16 μg/mL), ZICC (16 μg/mL), or MZCC (16 μg/mL). Following three PBS washes, cellular digestion was performed using trypsin. The collected cells were then suspended in 200 μL of 1× binding buffer and incubated for 15 minutes in darkness after adding 5 μL Annexin V-FITC and 10 μL propidium iodide. Apoptosis was then analyzed by flow cytometry.

Preparation of Rh B-Labeled MZCC

Rh B-labeled MZCC was prepared by direct mixing of Rh B labeled MCM and ZICC. Here, the Rh B labeled MCM was obtained by mixing Rh B and cell membrane directly and the combination between them was via physical absorption. The mixture was reacted at room temperature in the dark for 24 hours. Unreacted Rh B was removed by repeated washing with water via centrifugation until no detectable fluorescence signal remained in the supernatant. Finally, the Rh B-labeled MZCC was vacuum-dried to remove residual water.

Cellular Uptake of MZCC

Confocal laser scanning microscopy (CLSM) and flow cytometric analysis were employed to evaluate the intracellular accumulation of ZICC and MZCC in both CT26 and HT29 cell lines. For confocal imaging, cells were seeded in confocal

dishes at a density of 1×10^5 cells/well and incubated in McCoy's 5A medium (HT29 cells) or DMEM (CT26 cells), both supplemented with 10% FBS. Following cell attachment, the medium was aspirated and cells were washed with PBS. Following a 4-hour incubation at 37°C in serum-free medium containing either ZICC or MZCC (15 μg/mL), the cells underwent PBS washing to eliminate unbound compounds. Subsequently, cells were washed with PBS to remove unbound material, stained with DAPI to label nuclei, and given a final PBS wash. Fluorescent images were acquired using a confocal microscope.

Flow cytometry samples were prepared by plating cells at 10^5 cells/well in 24-well plates, with HT29 cells grown in McCoy's 5A and CT26 cells in DMEM, each medium containing 10% FBS. Following cell attachment, the medium was aspirated and cells were washed with PBS. Cells were then treated with ZICC/MZCC (15 μg/mL) in serum-free medium and incubated for 4 h at 37°C under 5% CO_2. Following incubation, cold PBS washes were conducted prior to cell detachment using 0.25% trypsin and isolation via centrifugation. The resulting cellular pellets were then prepared in suspension for analysis by flow cytometry.

Hemolytic Assay

A hemolysis assay was conducted on ZIF-8 to evaluate the biocompatibility and safety of the material. Anticoagulated blood was collected from experimental mice, and erythrocytes were isolated by centrifugation (5000 rpm, 5 min). The erythrocyte pellet underwent triple-washing with PBS (pH 7.4) and was subsequently reconstituted at 4% (v/v) in working solution. Subsequently, 1 mL of the diluted erythrocyte suspension was mixed with 1 mL of sample solutions at concentrations of 10, 50, 100, 200, and 250 μg/mL. PBS (1 mL) served as the negative control, and deionized water (1 mL) served as the positive control. Shaking samples at 150 rpm for 1 h (37°C) allowed for complete reaction. The resulting supernatant was then analyzed spectrophotometrically at 540 nm. Each group was analyzed in triplicate, the average absorbance was calculated, and the hemolysis rate was determined using the following formula:

$$HR\ (\%) = (OD\ sample - OD\ negative\ control) / (OD\ positive\ control - OD\ negative\ control) \times 100\%$$

In vivo Biodistribution Study

6–8 weeks old female athymic BALB/c mice were inoculated subcutaneously with 100 μL of PBS containing CT-26 cells (1×10^6) to construct colon tumor xenograft models. All procedures involving animals received ethical approval from the Henan Province Laboratory Animal Center and were conducted in strict accordance with international and national regulations on animal welfare (Guidelines for Ethical Review of Animal Welfare in Experiments GB/T 35892–2018), which were approved by the Institutional Animal Care and Use Committee of Zhengzhou University.

To evaluate the in vivo tumor targeting ability and biodistribution of ZICC and MZCC, fluorescence imaging was performed. Intravenous administration of RhB-labeled ZICC or MZCC was performed through the tail vein. Using an IVIS imaging system, in vivo fluorescence was monitored at scheduled intervals for 48 h. At 24 h post-injection, mice were sacrificed, and major organs (heart, liver, spleen, lung, kidney, intestine) along with tumors were excised for ex vivo imaging to examine the biodistribution of the RhB-loaded nanoparticles.

In vivo Antitumor Efficacy Studies

For studying the anticancer efficacy of MZCC in vivo, mice bearing tumors were received the following treatment every 4 days via *i.v.* injection (n = 5): (1) PBS; (2) CPT-11; (3) CPT-11+CCM; (4) ZIC; (5) ZICC; (6) MZCC (35 mg/kg body weight corresponding to CPT-11concentration). Over the 21-day observation period, tumor size progression and weight variations were systematically documented. Final analyses included colon length measurements and H&E-stained sections of both tumor and colon tissues across all experimental groups. Tumor volumetric calculations employed the standard formula: $(width^2 \times length)/2$.

Results and Discussion

Preparation and Identification of Biomimetic MZCC

To prepare MZCC, the first step involved a single reaction in an aqueous solution containing CPT-11, 2-methylimidazole and zinc nitrate hexahydrate to prepare CPT-11@ZIF-8 (named ZIC). A key advantage of this method is that both nanocarrier formation and drug loading occur within the same reaction system, resulting in an ultra-high drug-loading

capacity, these properties stem from the abundant binding sites on the ZIC nanocarriers. In the subsequent step, CCM was incorporated through physical adsorption, yielding CPT-11@CCM@ZIF-8 (named ZICC).

UV-vis spectroscopy, FT-IR, and XRD analyses collectively demonstrated the formation of ZICC. The appearance of distinct absorbance maxima around 220 and 390 nm in the UV-vis spectrum (Figure 2A) confirmed the successful synthesis. The FT-IR of ZICC revealed several characteristic bands of CPT-11 and CCM within the 1800–1200 cm^{-1} region, also confirming its incorporation into the ZIF-8 (Figure 2B). The XRD patterns of ZIC and ZICC exhibited identical characteristic peaks to those of ZIF-8, indicating that CPT-11 encapsulation and CCM loading did not substantially modify its crystalline architecture (Figure 2C). This strongly suggests that CPT-11 and CCM were efficiently incorporated into the ZIF-8 matrix without disrupting its structural integrity.

MR is a highly efficient endocytic receptor that mediates the cellular internalization and trafficking of mannose-terminated molecules or nanoparticles.[46] Given the overexpression of MR on CRC cells, mannosylation represents an effective targeting strategy for designing CRC-specific nanomedicine. Therefore, to improve the immune escape and homologous binding ability of the drug delivery system, the extracted CM was first functionalized by DSPE-PEG2000-MAN. To form the functionalized membrane (MCM), the synthesis involved combining an organic phase containing DSPE-PEG2000-MAN with an aqueous phase of buffer mixed with CM. The successfully preparation MCM was investigated by CLSM employing fluorophore Rhodamine B (Rh B) labeled DSPE-PEG2000-MAN and 3,

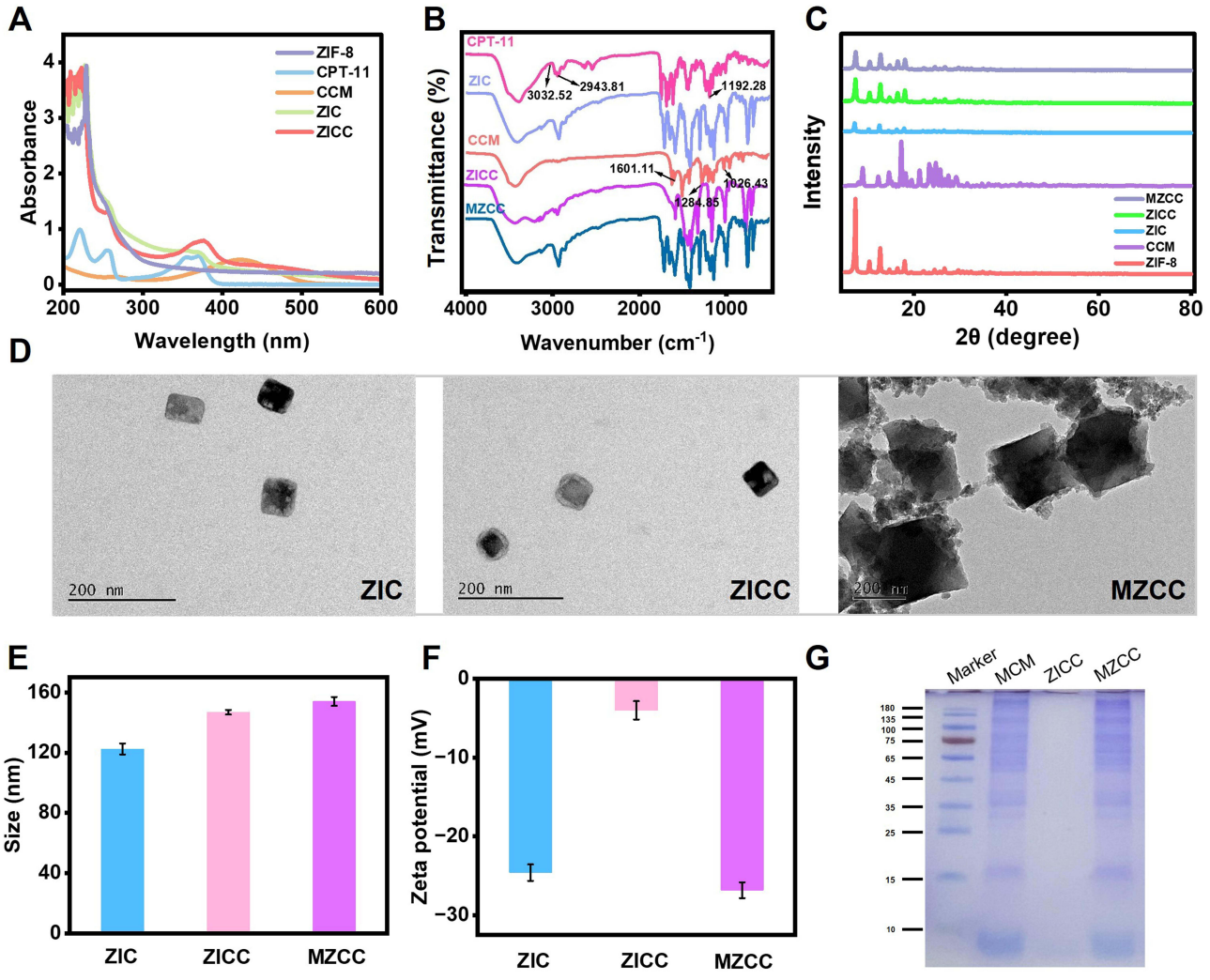

Figure 2 MZCC characterization. (**A**) UV−Vis absorbance spectra of ZIF-8, CPT-11, CCM, ZIC and ZICC. (**B**) FT-IR of CCM, CPT-11, ZIF-8, ZIC and ZICC. (**C**) XRD of CCM, ZIF-8, ZIC, ZICC and MZCC. (**D**) TEM image of ZIC, ZICC and MZCC. Scale bar: 100 nm. (**E**) Dynamic light scattering of ZIC, ZICC and MZCC. (**F**) Zeta potentials of ZIC, ZICC and MZCC. (**G**) SDS-PAGE of marker, MCM, ZICC and MZCC.

3-dioctadecyloxacarbocyanine perchlorate (Dio, Cell membrane staining agent) stained CM. As presented in Figure S1, the high degree of overlap between the signal of Rh B and Dio suggested the successful functionalization of CM. The obtained MCM was then extruded and sequentially coated onto the ZICC.

Microstructural characterization by TEM revealed significant differences between the nanoparticles. The MZCC formulation demonstrated a well-defined core-shell configuration with consistent lipid bilayer coverage (Figure 2D), in contrast to ZICC, confirming achievement of cancer cell membrane coating. Moreover, dynamic light scattering analysis confirmed the average particles size, yielding results consistent with TEM measurements (Figure 2E). Additionally, the zeta potential of MZCC decreased from −3.98 to −26.83 mV following MCM coating (Figure 2F). Sodium dodecyl sulfate-polyacrylamide gel electrophoresis (SDS-PAGE) analysis confirmed effective retention of the majority of associated membrane proteins within MZCC, whereas no protein signals were detected in ZICC, strongly indicating successful MCM coating of ZIC (Figure 2G). Additionally, the XRD pattern of MZCC also displayed the characteristic diffraction peaks of ZIF-8, with no discernible alterations. This consistency in XRD profiles demonstrates that the addition of MCM had no detrimental effect on the inherent crystallinity of ZIF-8 (Figure 2C).

Drug Loading and Release

The loading capacities of CPT-11 and CCM into the MZCC systems were evaluated via measuring the absorbance at 370 nm and 420 nm for CPT-11 and CCM, respectively. According to their standard curves (Figures S2 and S3), drug loading rates of 40.1% for CPT-11 and 13.2% for CCM were calculated. These results demonstrate that the prepared ZIF-8 possesses a high drug-loading capacity, making it a promising carrier for drug delivery. The cumulative release profiles of CPT-11 and CCM from the nanocarriers were investigated at different pH values (5.5, 6.4, and 7.4). According to their standard curves under different pH values (Figures S4-S9), the cumulative release at pH 7.4 was 21.2% for CPT-11 and 39.0% for CCM. More importantly, release significantly increased under acidic conditions (pH 5.5), reaching 65.3% for CPT-11 and 86.1% for CCM (Figures S10 and 11). This pH-responsive behavior indicates enhanced drug release in acidic environments. The pH-responsive properties of this nanocarrier system indicate its promising application for tumor-targeted drug delivery, where acidic microenvironment-triggered release of chemotherapeutic agents could minimize off-target toxicity in healthy tissues. The long-term stability of different formulations was also assessed in phosphate buffer saline and Dulbecco's Modified Eagle's medium. The result showed that MZCC was stable in both types of media for at least 7 days (Figure S12).

In vitro Targeting of MZCC

To verify our hypothesis that the MCM coating would confer MR-mediated targeting, we assessed the targeting ability of MZCC using laser confocal scanning microscopy (LCSM). MZCC nanoparticles were prepared for HT29 and CT26 cell lines (HT29 MCM@ZICC and CT26 MCM@ZICC, respectively) and incubated with their corresponding target cells. Rhodamine B (Rh B)-labeled MZCC exhibited red fluorescence, and nuclei were stained with DAPI (blue). As presented in Figure S13, limited MZCC uptake and minimal drug release were observed within the initial 2-hour incubation, as indicated by weak fluorescence. However, the red fluorescence intensity increased significantly by 4 hours, indicating efficient cellular uptake of MZCC. Moreover, LCSM images demonstrate that the red fluorescence intensity in both HT29 and CT26 cells incubated with MZCC was significantly higher than in cells incubated with uncoated ZICC (Figure 3A and B), indicating that MZCC is highly specifically targeted toward these cancer cells. Flow cytometry was used to quantitatively assess the differential cellular uptake of MZCC versus ZICC in CT26 cells, showing stronger fluorescence intensity in tumor cells treated with MZCC compared with ZICC (Figure 3C and D); this further validated the enhanced tumor-targeting ability of the MCM-coated nanoparticles.

Cytotoxicity of MZCC

Following confirmation of effective nanoparticle internalization and targeting, we evaluated the cytotoxic effects and apoptosis-inducing potential of various formulations using the 3-(4,5-dimethylthiazol-2-yl)-2,5-diphenyltetrazolium bromide (MTT)cell proliferation assay. Before studying the cytotoxicity of MZCC, we first assessed the cytotoxicity of ZIF-8 against human liver (7721), breast (MCF-7), and lung cancer cells (A549) using MTT assay. Incubation of 7721, A549, and MCF-7 cells with ZIF-8 (0–80 μg/mL) for 24 hours had negligible effects on cell viability (Figures S14-S16).

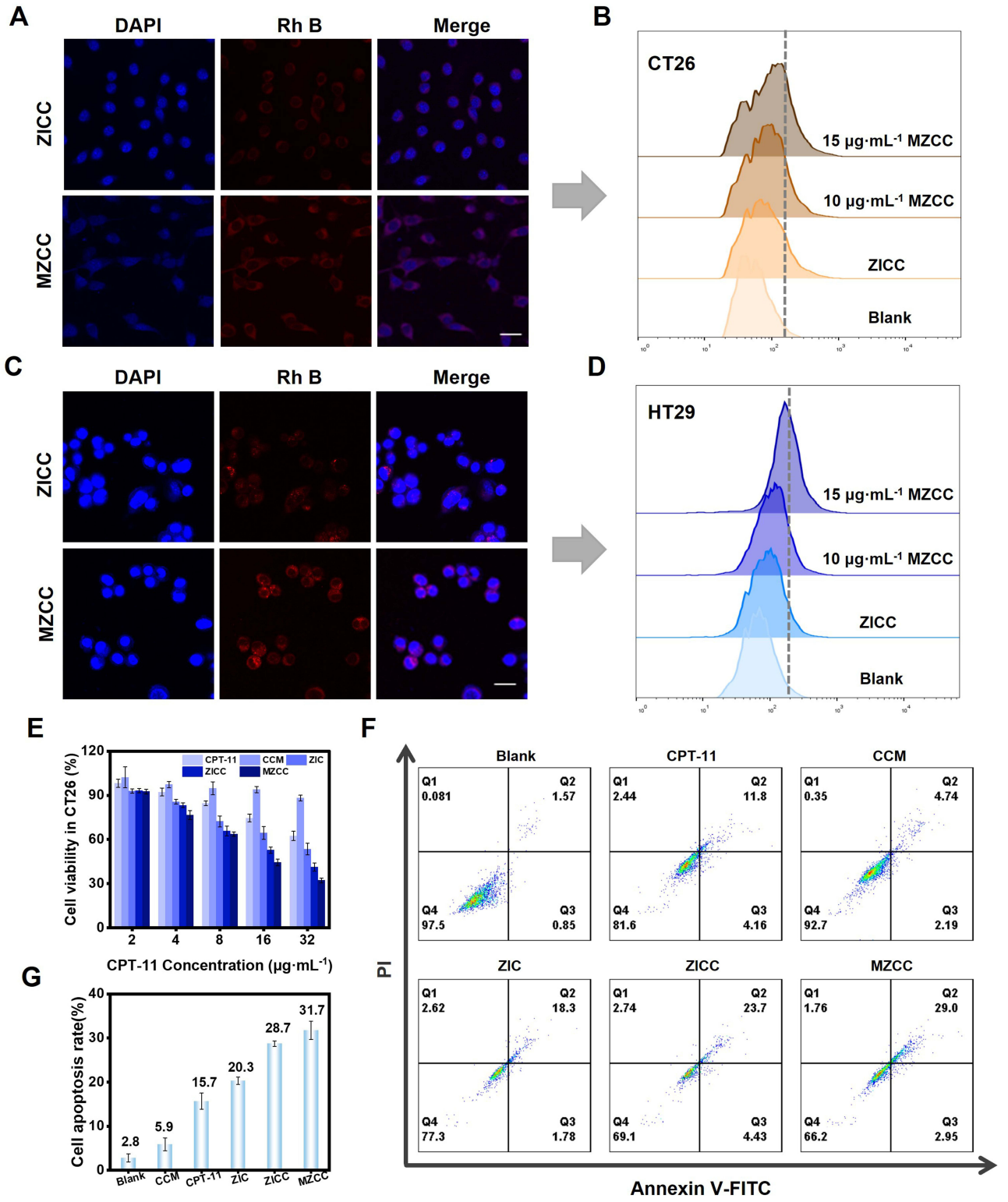

Figure 3 The targeting ability and Antitumor activity of MZCC in vitro. (**A**) Confocal fluorescent images of CT26 cells treated with MZCC. (**B**) Flow cytometry assay of labelling signals of MZCC for CT26. (**C**) Confocal fluorescent images of HT29 cells treated with MZCC. (**D**) Flow cytometry assay of labelling signals of MZCC for HT29. Scale bar: 25 μm. (**E**) Cell survival rate under different conditions. (**F**) Cell flow cytometry analysis of CT26 cells treated with different conditions. (**G**) Quantification of cell apoptosis rate of each group in (**F**).

Hemolysis tests have also been carried out to verify the biocompatibility biosecurity of ZIF-8. No hemolysis occurred even when the concentration of ZIF-8 was as high as 250 μg/mL (Figure S17). These results demonstrated the biocompatibility of ZIF-8 nanoparticles, supporting their suitability for constructing drug delivery systems.

The cytotoxicity of free CPT-11, free CCM, ZICC and MZCC was assessed in CT26 colon cancer cells (Figure 3E). At 16 μg/mL, free CPT-11 solution showed moderate inhibitory activity (76.0% ± 3.1% cell viability), while both ZICC and MZCC nanoparticles demonstrated significantly enhanced cytotoxicity. At 32 μg/mL, cell viabilities further decreased to 41.1% for ZICC and 32.8% for MZCC. Apoptosis induction was further analyzed by flow cytometry using Annexin V/PI double staining, with quadrants representing different populations as follows: Q1 (necrotic), Q2 (late apoptotic), Q3 (early apoptotic), and Q4 (viable) cells. The total apoptotic rate (Q2 + Q3) was significantly higher for MZCC (31.7%) compared with CPT-11 (15.7%), CCM (5.9%), ZIC (20.3%), and ZICC (28.7%) (Figure 3F and G). Consistent with MTT results, the MZCC group exhibited the highest apoptosis rate and lowest viable cell population (Q4), demonstrating superior antitumor efficacy. The enhanced therapeutic performance of MZCC can be attributed to homotypic targeting and immune evasion conferred by the biomimetic nano-delivery system, promoting efficient drug internalization, as well as synergistic anticancer activity mediated by CCM, which potentiates overall therapeutic outcomes.

In vivo Tumor Targeting Ability

CT26 tumor-bearing mouse models were established by subcutaneous injection of CT26 cells into the right flank. Mice were intravenously administered ZICC and MZCC nanoparticles (0.3 mg/mL in 200 μL), and biodistribution was monitored using real-time in vivo fluorescence imaging. At the tumor location, intense red fluorescence was detected immediately post-injection, showing a time-dependent enhancement in signal strength (Figure 4A and B). The signal peaked at approximately 12 h and demonstrated prolonged tumor retention; fluorescence intensity gradually decreased after 24 h but persisted beyond 48 h. This sustained retention may be facilitated by the MCM coating, which enhances immune evasion and targeting specificity. This prolonged circulation and tumor accumulation are expected to

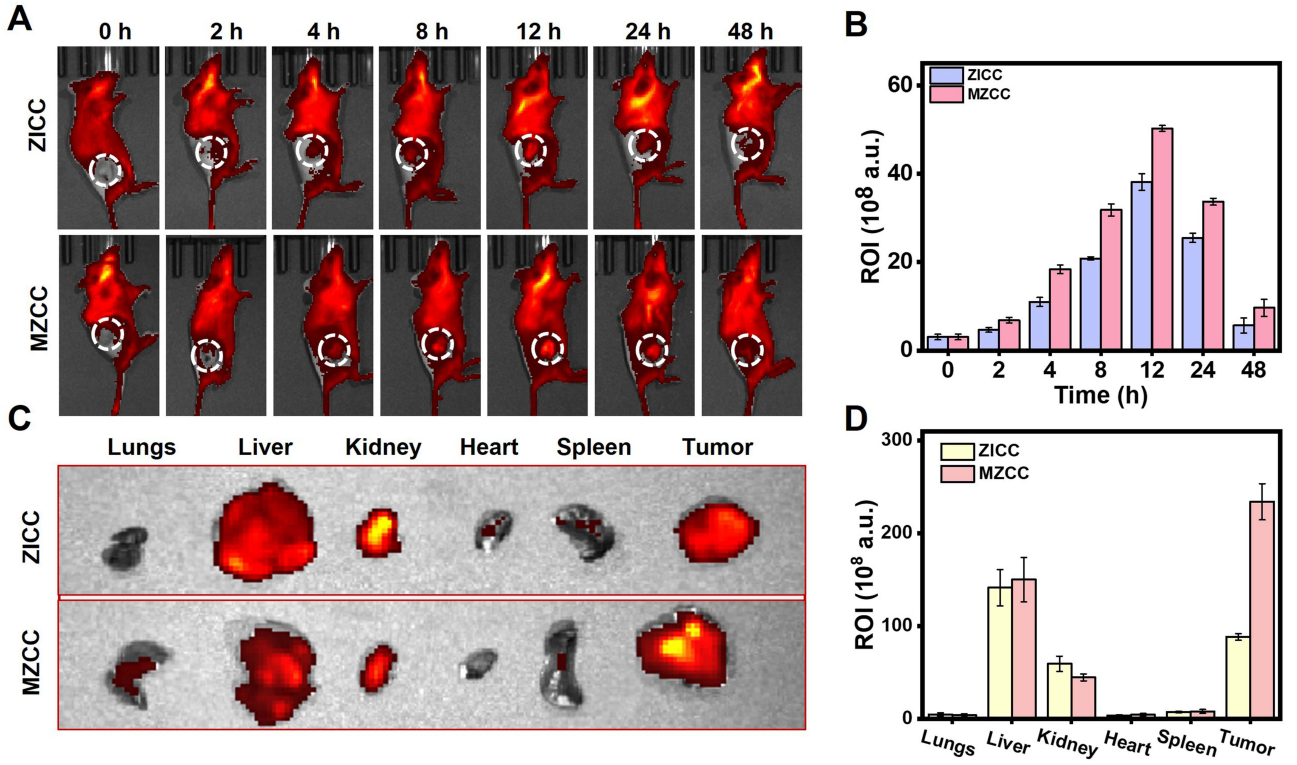

Figure 4 The targeting ability of MZCC in vivo. (**A**) Fluorescence imaging of the tumor site in mice at different time periods after injection of MZCC. (**B**) Statistics of fluorescence signal intensity of (**A**). (**C**) Ex vivo fluorescence images of main organs and tumors. (**D**) Statistics of fluorescence signal intensity of (**C**).

https://doi.org/10.2147/IJN.S558675

significantly improve therapeutic efficacy. Additionally, ex vivo imaging of harvested organs and tumors confirmed the preferential tumor accumulation of MZCC nanoparticles (Figure 4C and D).

Therapeutic Efficacy of MZCC in CT26 Mouse Model

Building upon promising tumor-targeting results, we evaluated the in vivo antitumor efficacy of various formulations in CT26 tumor-bearing BALB/c mice (Figure 5A). Female BALB/c mice bearing subcutaneous CT26 tumors, established by injecting 1×10^6 cells into the right flank, were randomly assigned to six groups (n = 5): PBS (control), CPT-11 (35 mg/kg), CPT-11+CCM, ZIC, ZICC, and MZCC. Treatments were administered intravenously every 4 day for 21 days, with tumor volumes monitored throughout. Tumors in the PBS group exhibited rapid growth, indicating limited therapeutic efficacy; in contrast, the MZCC group demonstrated the most potent tumor suppression, improving treatment antitumor efficacy by 2.3-fold compared with free irinotecan. While moderate inhibition was observed with ZICC and ZIC treatments (Figure 5B and C). Histological analysis corroborated these findings: H&E staining revealed the most extensive tumor necrosis in the MZCC group (Figure 5D), while TUNEL staining indicated the highest level of apoptosis (Figure 5E). These results collectively demonstrate that the MZCC formulation achieved enhanced antitumor efficacy through synergistic mechanisms.

Major Toxicity Reduction in the Gastrointestinal Tract with MZCC Treatment

Significantly reduced gastrointestinal side effects were observed in nanoparticle-treated mice. Histopathological analysis (Figure 6A) revealed that CPT-11 monotherapy induced substantial apoptosis of colonic crypt cells, while the CCM combination group maintained mucosal structural integrity through anti-inflammatory effects. CPT-11-induced intestinal

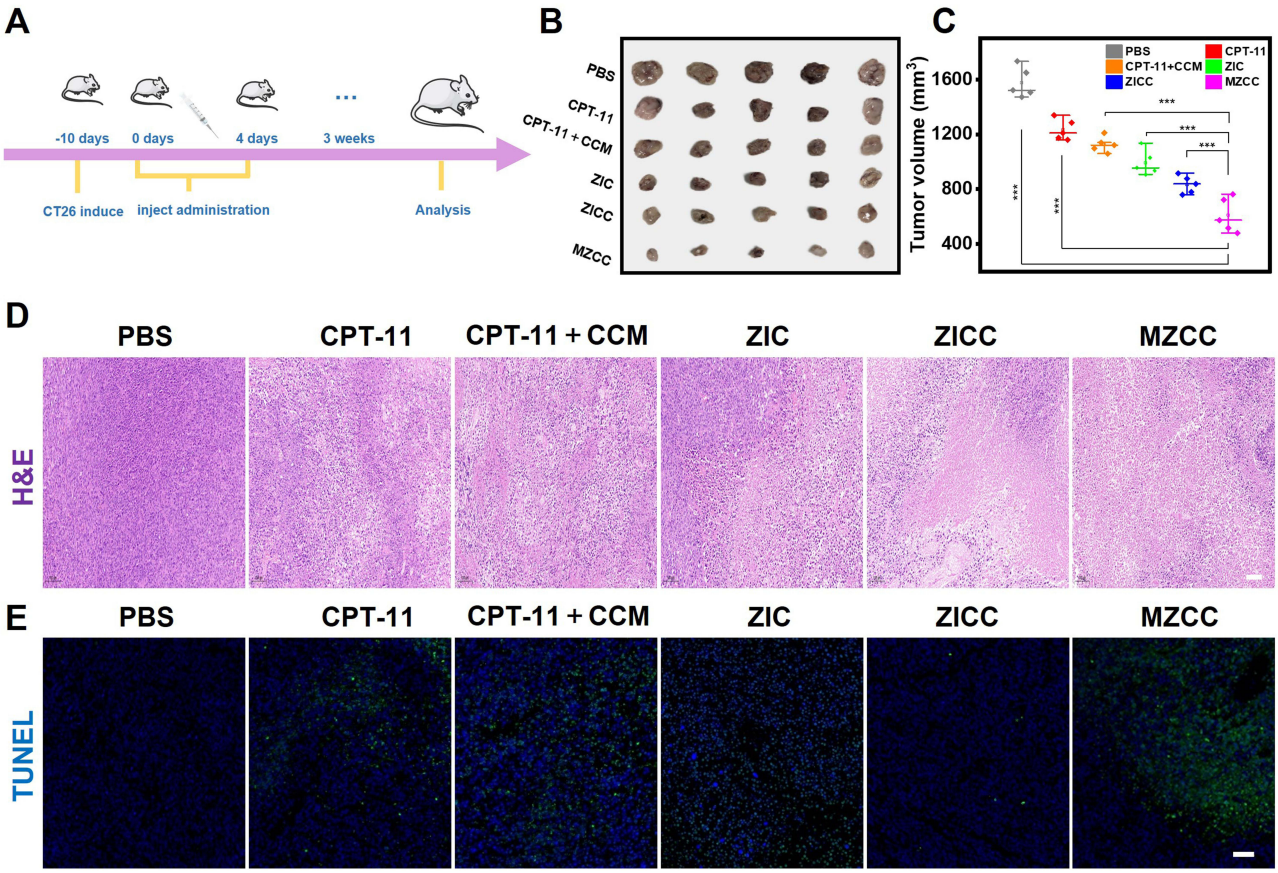

Figure 5 Anticancer activity in vivo. (**A**) Construction and treatment of BALB/c tumor-bearing CT26 mouse model. (**B**) Digital photographs of excised tumors after 21 days of treatment (n=5). (**C**) Relative tumor volume for each group. (**D**) H&E staining of tumor slices after 21 days of treatment. (**E**) TUNEL immunofluorescence images (blue, nucleus; green, apoptosis). Scale bar: 50 μm.

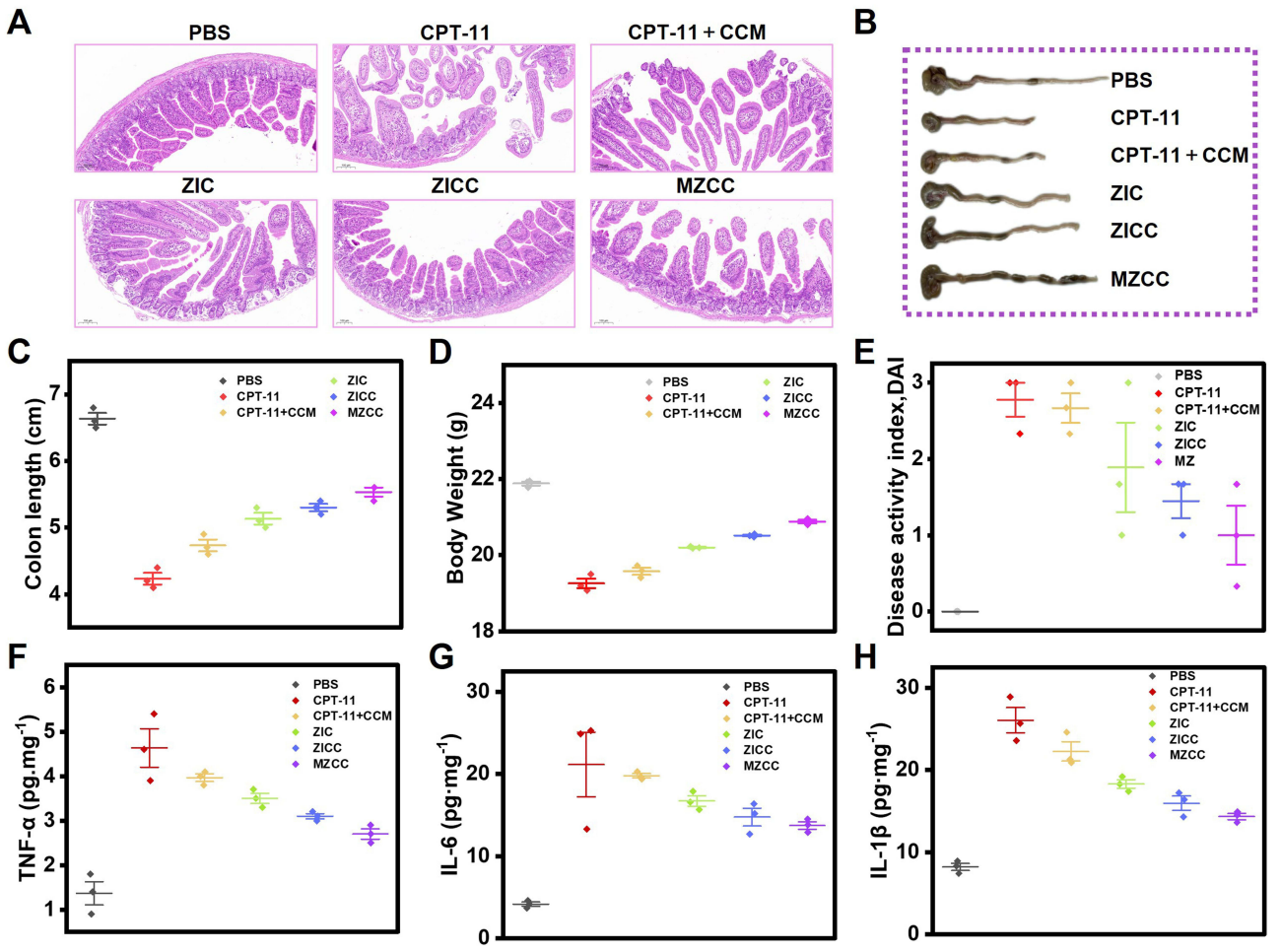

Figure 6 Gastrointestinal toxicity in vivo. (**A**) H&E staining of colon tissues after 21 days of treatment. (**B**) Images of excised colons after 21 days of treatment. (**C**) Statistics of colon length of (**C**). (**D**) Body weight of each group after 21 days of treatment. (**E**) Disease Activity Index of each group after 21 days of treatment. (**F**) The TNF-α expression level in colon tissues after 21 days of treatment. (**G**) The IL-6 expression level in colon tissues after 21 days of treatment. (**H**) The IL-1β expression level in colon tissues after 21 days of treatment.

damage was further evidenced by significant colon shortening. Examination of excised colons on day 21 confirmed that MZCC provided the best protection against colon shortening and histopathological damage with the colon length restored to 79% to normal (Figure 6B and C). This superior protection can be attributed to the lesion-targeting capability of MZCC's functionalized MCM membrane. CPT-11 and CCM combination therapy significantly recovered body weight (Figure 6D) and an improved Disease Activity Index (Figure 6E). Consistent with this, MZCC-treated groups exhibited a significant reduction in inflammatory cytokine levels within colon tissues; inflammation levels decreased by 55% compared with free CPT-11 (Figure 6F–H), indicating alleviated inflammation. Moreover, as shown in Figure S18, blood biochemical profiles showed no significant deviation from the control group, demonstrating the excellent biocompatibility of MZCC.

Conclusion

The present study successfully developed a pH-responsive drug delivery system based on MCM-coated ZIF-8 nanoparticles co-loaded with CPT-11 and CCM (MZCC) for targeted cancer therapy. Synthesis and characterization of MZCC confirm its potential as a sophisticated drug carrier, exhibiting high loading capacity, stability, and controlled release properties. In vitro release studies demonstrated that encapsulation within ZIF-8 significantly enhanced the pH-dependent release of both CPT-11 and CCM under acidic conditions, consistent with the tumor microenvironment. MTT assays revealed the potent anticancer efficacy of MZCC against CT26 cells, significantly reducing cell viability with observable

cytotoxic effects. This pH-responsive system holds promise for improving targeted drug delivery while minimizing off-target effects, representing a significant advancement in nanomedicine for cancer treatment. Crucially, in a CT26 mouse model, this delivery system demonstrated enhanced therapeutic efficacy and reduced toxicity through synergistic CPT-11 and CCM chemotherapy. Compared with other reported CPT-11 delivery systems, the proposed MZCC possessed obvious performance across three key parameters: drug loading, stability, and therapeutic index.[47,48] These biomimetic nanocarriers provide a valuable reference for developing tumor-targeted drug delivery systems and establish a theoretical foundation for novel cancer treatment strategies.

Acknowledgments

This work was supported by the National Natural Science Foundation of China (grant number 82470582, 22374136 and 22274143), Natural Science Foundation of Henan (grant number 232300421021, 242300421121 and 252300421019), the National Key Research and Development Program (2023YFF0714402), and Henan Provincial Special Program for Cultivating Clinical Medical Scientists (S20240021).

Disclosure

The authors have declared that no competing interest exists in this work.

References

1. Siegel RL, Kratzer TB, Giaquinto AN, et al. Cancer statistics, 2025. *CA Cancer J Clin*. 2025;75(1):10–45. doi:10.3322/caac.21871
2. Wang Y, Xie H, Ying K, et al. Tuning the efficacy of esterase-activatable prodrug nanoparticles for the treatment of colorectal malignancies. *Biomaterials*. 2021;270:120705. doi:10.1016/j.biomaterials.2021.120705
3. Yuan Y, Lin Q, Feng HY, et al. A multistage drug delivery approach for colorectal primary tumors and lymph node metastases. *Nat Commun*. 2025;16(1):1439. doi:10.1038/s41467-025-56768-z
4. Li Q, Geng S, Luo H, et al. Signaling pathways involved in colorectal cancer: pathogenesis and targeted therapy. *Signal Transduct Target Ther*. 2024;9(1):266. doi:10.1038/s41392-024-01953-7
5. Cui R, Zhou J, Yang W, et al. Ultrasound-triggered nanogel boosts chemotherapy and immunomodulation in colorectal cancer. *ACS Appl Mater Interfaces*. 2025;17(1):211–221. doi:10.1021/acsami.4c13358
6. Zhong H, Liang J, Xu X, et al. Hematoporphyrin-modified dendrimers combined immunoadjuvants for enhanced photoimmunotherapy of colorectal cancer. *ACS Appl Mater Interfaces*. 2025;17(17):25059–25070. doi:10.1021/acsami.5c02413
7. Bleiberg H. CPT-11 in gastrointestinal cancer. *Eur J Cancer*. 1999;35(3):371–379. doi:10.1016/s0959-8049(98)00423-7
8. Fuchs C, Mitchell EP, Hoff PM. Irinotecan in the treatment of colorectal cancer. *Cancer Treat Rev*. 2006;32(7):491–503. doi:10.1016/j.ctrv.2006.07.001
9. Ning ST, Lee SY, Wei MF, et al. Targeting colorectal cancer stem-like cells with Anti-CD133 antibody-conjugated SN-38 nanoparticles. *ACS Appl Mater Interfaces*. 2016;8(28):17793–17804. doi:10.1021/acsami.6b04403
10. Hecht JR. Gastrointestinal toxicity or irinotecan. *Oncology*. 1998;12(8 Suppl 6):72–78.
11. Mathijssen RH, van Alphen RJ, Verweij J, et al. Clinical pharmacokinetics and metabolism of irinotecan (CPT-11). *Clin Cancer Res*. 2001;7(8):2182–2194.
12. Xing J, Liu C, Zhang W, et al. Dual advantages of SN38 prodrug nanoassemblies overcome defects of irinotecan and SN38: enhanced stability and activatability. *Sci China Chem*. 2025;68(11):5960–5970. doi:10.1007/s11426-025-2760-2
13. Yu L, Qin X, Liang B, et al. Traditional Chinese medicine-based nanoformulations for enhanced photothermal therapy of cancer. *ACS Biomater Sci Eng*. 2025;11(2):694–709. doi:10.1021/acsbiomaterials.4c01612
14. Li S, Chen X, Shi H, et al. Tailoring traditional Chinese medicine in cancer therapy. *Mol Cancer*. 2025;24(1):27. doi:10.1186/s12943-024-02213-6
15. Liao Y, Zhao C, Pan Y, et al. Genetically engineered cellular nanoparticles loaded with curcuminoids for cancer immunotherapy. *Theranostics*. 2024;14(16):6409–6425. doi:10.7150/thno.99033
16. Alavi F, Majumder K, Ciftci ON. Designing curcumin particles with improved bioactivity and bioavailability using aerogels and supercritical fluid technology. *ACS Appl Mater Interfaces*. 2025;17(13):19263–19275. doi:10.1021/acsami.4c17001
17. Lu B, Zhong Y, Zhang J, et al. Curcumin-based ionic liquid hydrogel for topical transdermal delivery of curcumin to improve its therapeutic effect on the psoriasis mouse model. *ACS Appl Mater Interfaces*. 2024;16(14):17080–17091. doi:10.1021/acsami.3c17091
18. Liu X, Jiang J, Chan R, et al. Improved efficacy and reduced toxicity using a custom-designed irinotecan-delivering silicasome for orthotopic colon cancer. *ACS Nano*. 2019;13(1):38–53. doi:10.1021/acsnano.8b06164
19. Xu Z, Xie Y, Chen W, et al. Nanocarrier-based systems for targeted delivery: current challenges and future directions. *MedComm*. 2025;6(9):e70337. doi:10.1002/mco2.70337
20. Chen J, Xue F, Du W, et al. An endogenous H_2S-activated nanoplatform for triple synergistic therapy of colorectal cancer. *Nano Lett*. 2022;22(15):6156–6165. doi:10.1021/acs.nanolett.2c01346
21. Jones CW. Metal-organic frameworks and covalent organic frameworks: emerging advances and applications. *JACS Au*. 2022;2(7):1504–1505. doi:10.1021/jacsau.2c00376
22. Kumar S, Shukla MK, Sharma AK, et al. Metal-based nanomaterials and nanocomposites as promising frontier in cancer chemotherapy. *MedComm*. 2023;4(2):e253. doi:10.1002/mco2.253

23. Li C, Hang T, Jin Y. Atomically Fe-anchored MOF-on-MOF nanozyme with differential signal amplification for ultrasensitive cathodic electrochemiluminescence immunoassay. *Exploration*. 2023;3(4):20220151. doi:10.1002/EXP.20220151
24. Deng J, Wang K, Wang M, et al. Mitochondria targeted nanoscale zeolitic imidazole framework-90 for ATP imaging in live cells. *J Am Chem Soc*. 2017;139(16):5877–5882. doi:10.1021/jacs.7b01229
25. Huang S, Kou X, Shen J, et al. "Armor-Plating" enzymes with metal-organic frameworks (MOFs). *Angew Chem Int Ed*. 2020;59(23):8786–8798. doi:10.1002/anie.201916474
26. Xie Z, Liang S, Cai X, et al. O_2-Cu/ZIF-8@Ce6/ZIF-8@F127 composite as a tumor microenvironment-responsive nanoplatform with enhanced photo-/chemodynamic antitumor efficacy. *ACS Appl Mater Interfaces*. 2019;11(35):31671–31680. doi:10.1021/acsami.9b10685
27. Yang X, Tang Q, Jiang Y, et al. Nanoscale ATP-responsive zeolitic imidazole framework-90 as a general platform for cytosolic protein delivery and genome editing. *J Am Chem Soc*. 2019;141(9):3782–3786. doi:10.1021/jacs.8b11996
28. Guan Q, Zhou LL, Li YA, et al. Diiodo-bodipy-encapsulated nanoscale metal-organic framework for ph-driven selective and mitochondria targeted photodynamic therapy. *Inorg Chem*. 2018;57(16):10137–10145. doi:10.1021/acs.inorgchem.8b01316
29. Tian R, Zhang Z, Song L, et al. A diselenide MOF-based nanomotor dual-driven by carbon monoxide and near-infrared-II light for multimodal tumor-targeted therapy. *Sci China Chem*. 2025;68(5):1952–1969. doi:10.1007/s11426-024-2331-y
30. Shen N, Zhao W, Chu H, et al. Targeted delivery and controlled release of polymeric nanomedicines for tumor therapy. *Fundam Res*. 2025;5(4):1349–1368. doi:10.1016/j.fmre.2025.01.011
31. Maddigan NK, Tarzia A, Huang DM, et al. Protein surface functionalisation as a general strategy for facilitating biomimetic mineralisation of ZIF-8. *Chem Sci*. 2018;9(18):4217–4223. doi:10.1039/c8sc00825f
32. Chen TT, Yi JT, Zhao YY, et al. Biomineralized metal-organic framework nanoparticles enable intracellular delivery and endo-lysosomal release of native active proteins. *J Am Chem Soc*. 2018;140(31):9912–9920. doi:10.1021/jacs.8b04457
33. Lin S, Cui J, Li X, et al. Modified ZIF-8 nanoparticles for targeted metabolic treatment of acute spinal cord injury. *ACS Appl Mater Interfaces*. 2024;16(12):14503–14509. doi:10.1021/acsami.3c13984
34. Li SY, Cheng H, Xie BR, et al. Cancer cell membrane camouflaged cascade bioreactor for cancer targeted starvation and photodynamic therapy. *ACS Nano*. 2017;11(7):7006–7018. doi:10.1021/acsnano.7b02533
35. Miao C, Shen Y, Lang Y, et al. Biomimetic nanoparticles with enhanced rapamycin delivery for autism spectrum disorder treatment via autophagy activation and oxidative stress modulation. *Theranostics*. 2024;14(11):4375–4392. doi:10.7150/thno.95614
36. Wang KN, Li ZZ, Zhou K, et al. Cell membrane-coated nanoparticles for dental, oral, and craniofacial diseases. *Research*. 2024;7:0478. doi:10.34133/research.0478
37. Zhang S, Li R, Xu Y, et al. Engineered bacteria: strategies and applications in cancer immunotherapy. *Fundam Res*. 2024;5(3):1327–1345. doi:10.1016/j.fmre.2024.11.001
38. Harris JC, Scully MA, Day ES. Cancer cell membrane-coated nanoparticles for cancer management. *Cancers*. 2019;11(12):1836. doi:10.3390/cancers11121836
39. Liu W-L, Zou M-Z, Qin S-Y, et al. Recent advances of cell membrane-coated nanomaterials for biomedical applications. *Adv Funct Mater*. 2020;30(39):2003559. doi:10.1002/adfm.202003559
40. Yang Y, Liu Q, Wang M, et al. Genetically programmable cell membrane-camouflaged nanoparticles for targeted combination therapy of colorectal cancer. *Signal Transduct Tar*. 2024;9(1):158. doi:10.1038/s41392-024-01859-4
41. Li L, Wang F, Zhu D, et al. Engineering exosomes and exosome-like nanovesicles for improving tissue targeting and retention. *Fundam Res*. 2024;5(2):851–867. doi:10.1016/j.fmre.2024.03.025
42. Wu H, Cao G, Liu M, et al. Tumor cell membrane biomimetic liposomes-coated oncolytic viruses to target the homotypic tumor and augment the antitumor efficacy. *Chin Chem Lett*. 2025;36(7):110493. doi:10.1016/j.cclet.2024.110493
43. Zhao P, Yin W, Wu A, et al. Dual-targeting to cancer cells and M2 macrophages via biomimetic delivery of mannosylated albumin nanoparticles for drug-resistant cancer therapy. *Adv Funct Mater*. 2017;27(44):1700403. doi:10.1002/adfm.201700403
44. Mizuta Y, Maeda H, Ishima Y, et al. A mannosylated, PEGylated albumin as a drug delivery system for the treatment of cancer stroma cells. *Adv Funct Mater*. 2021;31(43):2104136. doi:10.1002/adfm.202104136
45. Ding B, Chen H, Tan J, et al. ZIF-8 nanoparticles evoke pyroptosis for high-efficiency cancer immunotherapy. *Angew Chem Int Ed*. 2023;62(10):e202215307. doi:10.1002/anie.202215307
46. Feng H, Feng Y, Lin L, et al. Mannose receptor-mediated carbon nanotubes as an antigen delivery system to enhance immune response both in vitro and in vivo. *Int J Mol Sci*. 2022;23(8):4239. doi:10.3390/ijms23084239
47. Wang T, He W, Du Y, et al. Redox-sensitive irinotecan liposomes with active ultra-high loading and enhanced intracellular drug release. *Colloids Surf B Biointerfaces*. 2021;206:111967. doi:10.1016/j.colsurfb.2021.111967
48. Jafernik K, Ładniak A, Blicharska E, et al. Chitosan-based nanoparticles as effective drug delivery systems-A review. *Molecules*. 2023;28(4):1963. doi:10.3390/molecules28041963